Vol.2, No.2, Page 116- 123, 2024 https://doi.org/10.59628/jast.v2i2.874 ISSN 2958-9568 JAST

SUN PUBLISHER

مجلة جامعة صنعاء للعلوم التطبيقية والتكنولوجيا

Sana'a University Journal of Applied Sciences and Technology

https://journals.su.edu.ye/index.php/jast/

Synthesis and Characterization of (CdO- CuO-Co_3O_4) Mixed Metal Oxides Nanocomposite

Shadha Nasser Aziz[1,3] *, A.M. Abdulwahab[2] † and Thana Shuga Aldeen[1]

[1]**Department of Physics, Faculty of Science, University of Sana'a, Sana'a, Yemen,**
[2]**Physics Department, Faculty of Applied Science, Thamar University, Dhamar 87246, Yemen,**
[3]**Al-Darb Community College, Dhamar, Yemen.**

*Corresponding author: Shd.Aziz@su.edu.ye
†Corresponding author: abduhabdulwahab@yahoo.com

Abstract

The main goals of this study are to synthesize a mixed metal oxide nanocomposite (NC), CdO-CuO-Co_3O_4, and to analyze its structural, morphological, optical, and electrical properties using X-ray diffraction (XRD), total reflection X-ray fluorescence (TXRF), transmission electron microscopy (TEM), diffuse reflectance spectroscopy (DRS), and DC electrical resistivity. According to the XRD analysis, CuO nanoparticles (NPs) have a monoclinic structure, while CdO and Co_3O_4 (NPs) have cubic structures. The TEM images revealed a decrease in the particle size of CdO-CuO-Co_3O_4 (NC) compared with that of the NPs. The optical properties of CdO-CuO-Co_3O_4 (NC) were examined using a DRS in the wavelength range of 400-700 nm. The DC electrical resistivity results showed the semiconducting electrical behaviors of the samples.

Article Info

Keywords:
CdO-CuO-Co_3O_4 nanocomposites (NC), TEM, Optical band gap, Electrical resistivity

Article History:
Received: 11-February-2024,
Revised: 12-March-2024,
Accepted: 18-March-2024,
Available online: 5 May 2024

1. INTRODUCTION

The primary focus of current nanotechnology research is to synthesize new nanomaterials, which have a variety of intriguing applications in fields such electrochemistry, biomedicine, catalysis, cosmetics, electronics, and optical devices, as well as in energy science, mechanics, food technology, healthcare, sensors, textile technology, space technology, and pharmaceuticals [1–5]. The synthesis of multi-metal oxides nanocomposites involves mixing more than one oxide at the nanometer scale. These nanocomposites exhibit properties that vary according to the concentration of each constituent oxide in the mixture [1]. The various properties of individual oxides can be greatly improved by mixing different metal oxides (MOs) to form new NCs, which would then improve performance in a variety of technological applications. These characteristics of nanocomposites may play a significant role in a variety of applications, including solar cells, fuel cells, UV detectors, battery materials, gas sensors, photovoltaic devices, and biomedicine. It is common knowledge that new composite materials, which have recently attracted interest in technology, can be produced by combining various compounds with exceptional dielectric characteristics. In addition, a new stage can significantly improve the electronic properties of the resulting composite material. A variety of methods can be used to synthesize nanocomposites, including solid-state mixing [6], electrochemical methods [7], hydrothermal growth [8], sonochemistry [9], the sol-gel technique [10], high-pressure synthesis [11], glycine nitrate combustion [12], co-precipitation methods [13], and thermal evaporation [14]. Through these, the co-precipitation method is utilized because it is effective, simple, and fast; it also reduces the growth of the temperature and does not cost [15]. The special chemical, electrical, and optical properties of cadmium oxide nanoparticles (CdO NPs), an n-type semiconductor with a 2–2.7 eV direct optical bandgap, make it an ideal material for photocatalytic applications [16–19]. Copper oxide (CuO NPs), a p-type semiconductor with a small bandgap ($1.2 - 2.4\ eV$), has significant applications in the development of superca-

pacitors, near-infrared filters, magnetic storage media, sensors, catalysis, and semiconductors [20–23]. Owing to their low price, environmental friendliness, simplicity of preparation, and exceptional chemical and physical stability, cobalt oxide (Co_3O_4 NPs), a p-type semiconductor with a bandgap of $1.2 - 3.34\ eV$, has gained more attention in recent years for its effectiveness in the photodegradation of dye pollutants. Additionally, Co_3O_4 NPs, which are used in various applications such as gas sensors and supercapacitors, have exceptional optical, electrical, and magnetic properties [24–26]. The combination of magnetic Co_3O_4 with semiconducting CdO and CuO could result in interesting magnetic and electronic behaviors suitable for applications such as sensors or electronic devices. In this study, CdO, CuO, Co_3O_4 (NPs), and CdO-CuO-Co_3O_4 (NC) were synthesized using the co-precipitation method. The samples were characterized by XRD, TXRF, TEM, and DRS, and their DC electrical conductivities were studied.

2. EXPERIMENTAL PROCEDURE

Distilled water (DW), cadmium nitrate terthydrate ($Cd(NO_3)_2.4H_2O$) (99%) (HIMEDIA), copper nitrate trihydrate ($Cu(NO_3)_2.3H_2O$) (98%) (HIMEDIA), cobalt nitrate hexahydrate ($Co(NO_3)_2.6H_2O$) (98%) (HIMEDIA), and Sodium hydroxide NaOH (98%) (HIMEDIA) were used in this research.

3. SYNTHESIS OF CDO-CUO-CO_3O_4 NANOCOMPOSITE

To synthesize CdO-CuO-Co_3O_4 (NC), a 0.03M precursor solution with a Cd:Cu:Co molar ratio of 1:1:1 was prepared by weighing 7.71g of $Cd(NO_3)_2.4H_2O$, 6.04 g of $Cu(NO_3)_2.3H_2O$, and 7.27g of $Co(NO_3)_2.6H_2O$ and dissolving them all in 300 ml of distilled water under constant stirring for 10 min at ambient temperature. Then, a 0.1M NaOH solution was added dropwise to the mixed precursor solution to adjust its pH value to 7 while continuously stirring for 1 h. A precipitate was formed immediately. The precipitate was collected by filtration, washed several times with distilled water, and then dried at 100 ^oC for 1 h. Therefore, it was ground using a mortar and pestle to obtain a fine powder. Finally, the powder was annealed at 500 °C for 2 h to obtain NC. In a manner similar to that for the composites, individual pure oxides (CdO, CuO, and Co_3O_4) were separately prepared using the corresponding salt. Similarly, individual CdO, CuO, and Co_3O_4 (NPs) were produced using the co-precipitation technique, where 7.71g of $Cd(NO3)_2.4H_2O$ (or 6.04g of $Cu(NO3)_2.3H_2O$ or 7.27 g of $Co(NO3)_2.6H_2O$) and 0.1 M NaOH were added to 100 ml of distilled water. Finally, brown of CdO (NPs) and black of CuO (NPs),Co_3O_4(NPs) and nanocomposite powders were formed as shown in Fig. 1.

4. CHARACTERIZATIONS

The structural properties of the prepared CdO, CuO, Co_3O_4 and CdO-CuO-Co_3O_4 (NC) were investigated using XRD technique (XD-2 X-ray diffractometer using CuK_α (λ= 0.154 nm) at 36 kV and 20 mA, China). The concentrations of each element in the samples were measured using (TXRF) (xrf, S8 tiger, German) from the Yemeni Geological Survey and Minerals Resources Board. The nanoparticle size was determined using transmission electron microscopey TEM (JEM-2100, Japan) transmission electron microscope. The used particle size of The TEM was evaluated using the Image-J software. Using DR spectra over the wavelength range of 400–700 nm (Model: JASCO, V-750, Japan), the diffused reflectances of CdO, CuO, Co_3O_4 (NPs) and, CdO-CuO-Co_3O_4 (NC) were measured. The conductivities of the compounds were measured by a Keithley-6517B electrometer, (USA).

5. RESULTS AND DISCUSSION

5.1. Structural analysis

The XRD patterns of the metal oxides CdO, CuO, Co_3O_4 (NPs), and CdO-CuO-Co_3O_4 (NC) are shown in Fig. 2. The XRD pattern of the NPs emphasized the presence of cubic CdO, Co_3O_4, and monoclinic CuO. The diffraction peaks matched well with the typical JCPDS Card No (01–1049) of CdO, (048-1548) of CuO, and (042-1467) of Co_3O_4. Diffraction peaks of CdO, CuO, and Co_3O_4

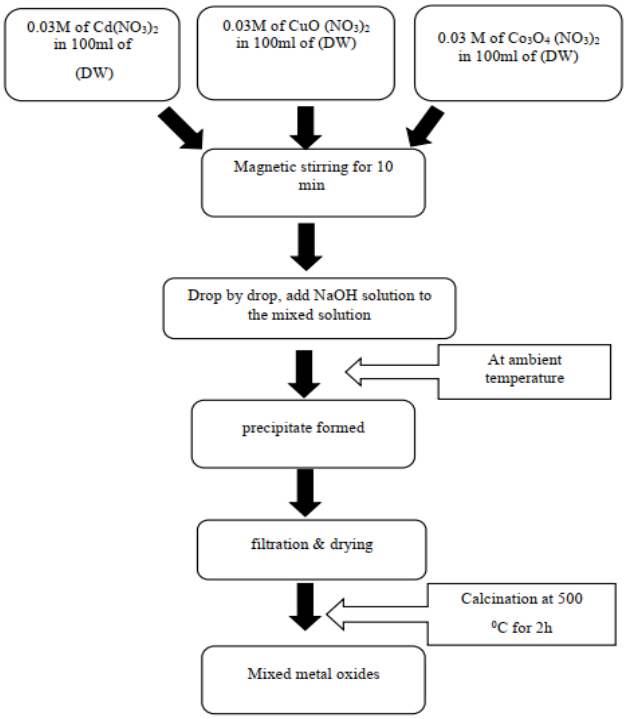

Figure 1. Flowchart for the preparation of CdO, CuO, Co_3O_4 (NPs) and CdO-CuO-Co_3O_4 (NC)

can be observed in the multi-metal oxide composite pattern, as shown in Fig. 2. Owing to the close diffraction angles, some of the diffraction peaks of the metal oxides in the XRD model of the composite were shifted. The peaks of CuO and Co_3O_4 in CdO-CuO-Co_3O_4 (NC) were higher intensity than those of CdO. Scherrer's equation,

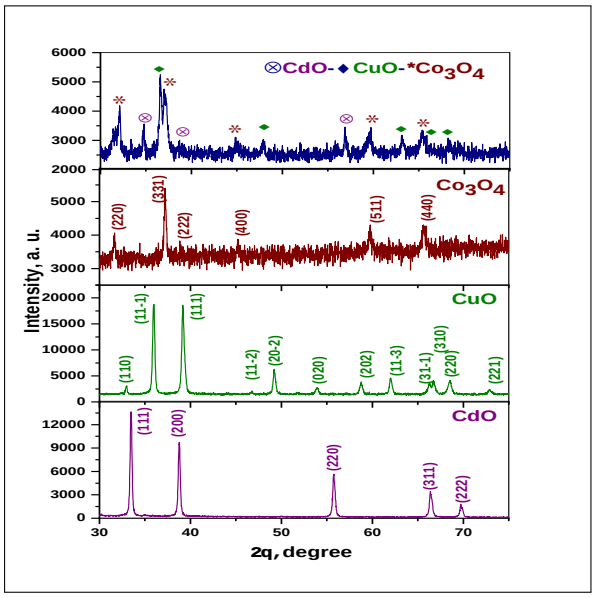

Figure 2. Flowchart for the preparation of CdO, CuO, Co_3O_4 (NPs) and CdO-CuO-Co_3O_4 (NC)

as expressed in Eq. (1) [27], was used to calculate the average crystallite size (D, nm) of CdO,CuO,Co_3O_4 (NPs) and CdO-CuO-Co_3O_4 (NC).

$$D = \frac{0.9\lambda}{\beta\ Cos\ \theta}, \tag{1}$$

where λ is the wavelength of the X-ray used, β is the full-width at half maximum intensity (FWHM) (in radians), and θ is the diffraction angle.

Table 1 shows that the calculated value of D for CdO was greater than that for CuO and Co_3O_4. The crystallite sizes (D) of CdO, CuO, and Co_3O_4 in the nanocomposite decreased when compared to their size as nanoparticles, which indicates a decrease in the crystal growth of the nanocomposite. The micro-strain (ϵ) and dislocation density (δ) in the crystals were calculated using the relationships (2,3) [28]. The average crystallite size, dislocation density, and micro-strain for CdO, CuO, Co_3O_4 (NPs), and CdO-CuO-Co_3O_4 (NC) are listed in Table 1.

$$\epsilon = \frac{\beta}{4\tan\ \theta}, \tag{2}$$

$$\delta = \frac{1}{D^2}. \tag{3}$$

It is obvious that combining CdO, CuO, and Co_3O_4 (NPs) increases the dislocation density and decreases the grain size of the (NC). This result agrees with Munawar *et al* [29]. The decrease in the crystalline sizes is often associated with a higher density of defects and dislocations within the crystal lattice. These defects contribute to the microstrain by disrupting the regular atomic arrangement.

Table 1. The values of D and ϵ of CdO, CuO, and Co_3O_4 (NPs) as well as CdO-CuO -Co_3O_4 (NC) determined using XRD analysis.

	Samples	$D(nm)$	$\varepsilon \times 10^{-3}$	$\delta(nm^{-2}) \times 10^{-3}$
Single	*CdO*	*37.73*	*1.7*	**0.7**
metal	*CuO*	*30.76*	*4.1*	**1.1**
oxides	*Co_3O_4*	*32.8*	*6.4*	**0.9**
CdO-CuO-	*CdO*	*32.26*	*3.8*	**0.9**
Co_3O_4	*CuO*	*24.9*	*4.9*	**1.6**
Mixed metal oxides	*Co_3O_4*	*16.1*	*13.1*	**3.9**

5.2. Elemental Analysis

The results of the elemental chemical analysis of the prepared samples carried out suing TXRF are listed in Table 2. CdO, CuO, and Co_3O_4 (NPs) constitute the majority of nanocomposite materials. Some impurities, including P, S, Ca, Fe, and,Si, were present in trace amounts. This result is consistent with that of Jianfeng *et al* [30].These results confirmed the purity of the prepared samples.

Table 2. TXRF analysis of CdO-CuO-Co_3O_4 (NC).

Compound	Wt %	Elemental	Wt %
CuO	42.29%	Cu	39.14%
Co_3O_4	39.88%	Co	31.09%
CdO	17.38%	Cd	11.13%
-	-	O	18.19%

5.3. TEM ANALYSIS

The size and morphology of the synthesized nanoparticles and nanocomposites were determined using TEM, and the Image-J program was used to determine the particle sizes. TEM images of CdO, CuO, Co_3O_4 (NPs) and CdO- CuO- Co_3O_4 (NC) are shown in Fig.3(a). Spherical particles with an average size of $60.8\ nm$,$70.7\ nm$ and $33.4\ nm$ were observed for CdO, CuO and Co_3O_4 (NPs) respectively. For the composite, the particles were agglomerated, and a mixture of particles, most of which were spherical and nanorod-shaped, could be detected. The average particle size of the composite was found to be 11.4 nm. The particle size of CdO-CuO-Co_3O_4 (NC) decreased compared to that of (NPs), which is in good agreement with previous studies [31]. The TEM results are consistent with the XRD results, which showed a reduction in the crystallite size of (NC) compared to that (NPs).Histogram graphs were shown in Fig. 3 (b).

5.4. OPTICAL STUDIES

5.4.1. Optical Band gap energy

The optical characteristics of CdO, CuO,Co_3O_4 (NPs, and CdO-CuO-Co_3O_4 (NC) materials were evaluate using diffuse reflectance spectroscopy. The reflectance spectra of the samples in the wavelength range of 400-700 nm are shown in Fig. 4 as a function of wavelength. The reflectance spectrum gradually decreased with increasing wavelength and then stabilized at a nearly constant value, except for CdO, where the reflection was at a constant low value and then increased with increasing wavelength. The absorbance was calculated by converting the measured reflectance using the Kubelka-Munk Eq. (4) [32].

$$F(R) = \frac{(1-R)^2}{2R}, \tag{4}$$

where R is the diffuse reflectance $(\%)$, and F (R) is the Kubelka-Munk function corresponding to the absorbance.

The following calculations were performed using the modified K-M equation to determine the material's band gap energy (E_g) and the type of optical transition between the valence band (VB) and conduction band (CB):

$$(F(R)\,hv) = A(E - E_g)^n, \tag{5}$$

where the constant A depend on the transition possibility and measures the disorder of the material and band tailing, $(E{=}hv)$ is the photon energy, and the exponent factor n is related to the nature of the optical transition and is equal to 1/2 for allowed direct optical transitions [32]. The band-gap values were determined by extrapolating the linear region of the plot to E= 0. Tauc plots of $(F(R)\,E)^2$ vs E. The optical band gaps (E_g) of CdO, CuO, Co_3O_4 (NPs), and CdO-CuO-Co_3O_4 (NC) are shown in Fig. 5 and Table 3.

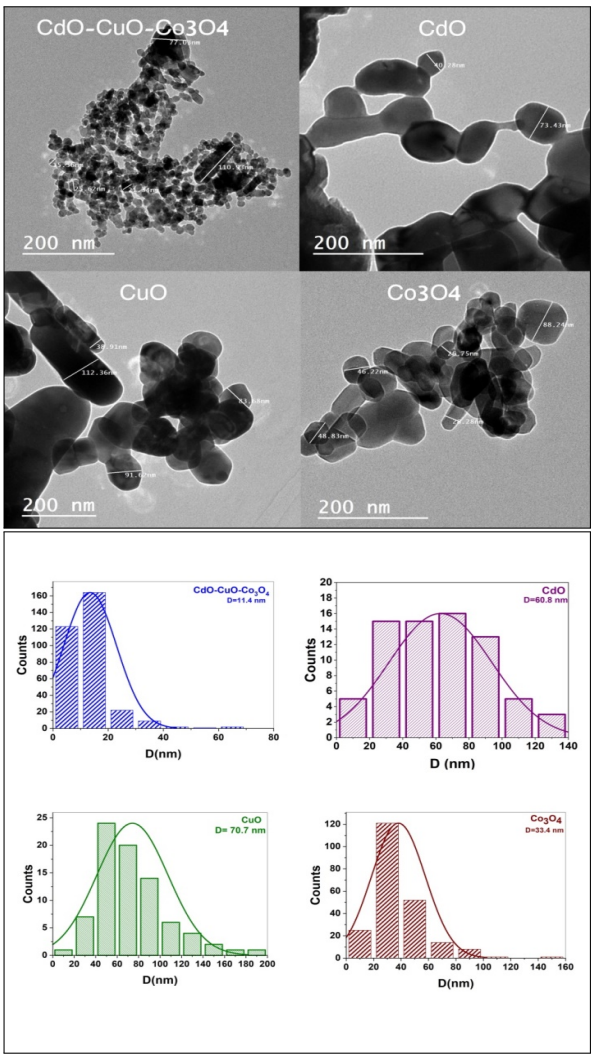

Figure 3. (a). TEM image of the CdO,CuO,Co3O4 (NPs) and CdO-CuO-Co3O4 (NC). (b).Histograms calculated from TEM images CdO,CuO,Co3O4 (NPs) and CdO-CuO-Co3O4 (NC)

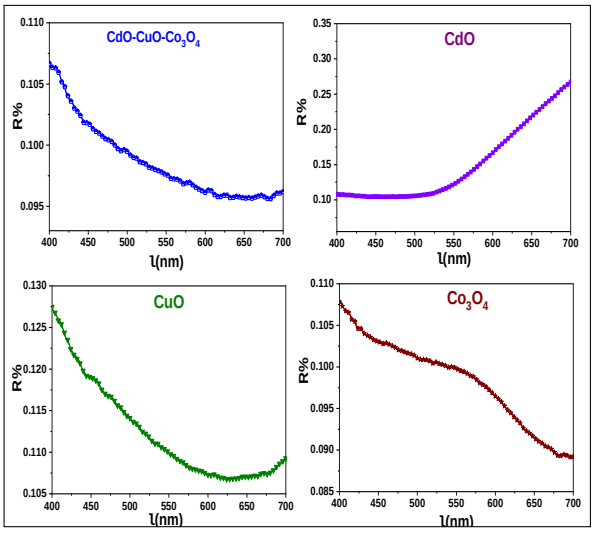

Figure 4. Difuse refectance spectrum (R%) of the CdO,CuO,Co_3O_4 (NPs) and CdO-CuO-Co_3O_4 (NC)

Co_3O_4 (NP) has two bandgaps at 1.4 eV and 1.16 eV

Table 3. Optical energy band gaps (E_g) for CdO, CuO, Co_3O_4 (NPs) and CdO-CuO-Co_3O_4 (NC)

Sample	$E_g(eV)$
CdO	2
CuO	1.5
Co_3O_4	1.16 &1.4
CdO-CuO-Co_3O_4	1.24

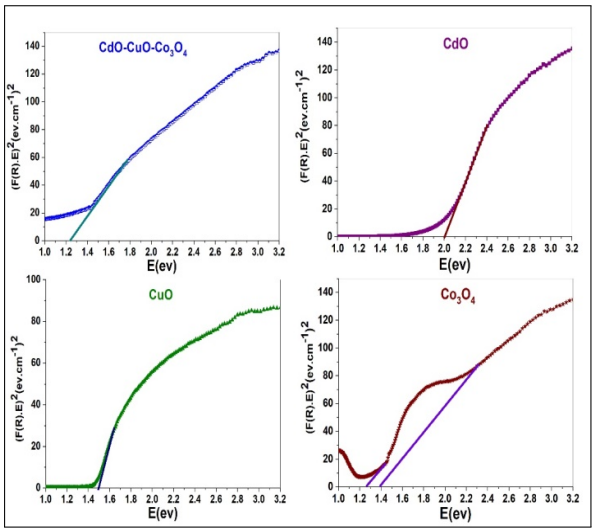

Figure 5. The plot of $(F(R)\,h\nu)^2$ vs E(ev) for direct band gap

due to $O_{2-} \rightarrow Co_{2+}$ and $O_{2-} \rightarrow Co_{3+}$ charge transfer transition respectively [25]. The optical band gap of CdO-CuO-Co_3O_4 (NC) is lower than that of (NPs). This result was supported by the electrical resistivity measurements discussed below. The band-gap value of NC (1.24 eV) falls within the range of a narrow band-gap semiconductor, which is consistent with the results of previous studies [18, 33–35]. Materials with such band gaps have potential applications in photovoltaics, photocatalysis, and ensors.

5.4.2. Extinction coefficient and refractive index

The extinction coefficient (k) Eq. (6), also known as the absorption index, measures the quantity of light lost in a test material per unit distance due to absorption and scattering. It is possible to calculate k using the optical absorption coefficient (α) and event photon wavelength (λ) [29].

$$k = \frac{\alpha\lambda}{4\pi}. \tag{6}$$

Eq. (7) can be used to determine the refractive index (n) of a crystalline solid from its reflectance (R) [36].

$$R = \frac{(n-1)^2+k^2}{(n+1)^2+k^2}, \tag{7}$$

Where, k: is the extinction coefficient. Because of the small size of k, Eq. (8) can be changed to [36]:

$$n = \frac{1+\sqrt{R}}{1-\sqrt{R}}. \tag{8}$$

According to Fig. 6(a) and 6(b), respectively, the n and k as functions of the photon energy supply, an analysis of the local field, and the ion's electronic polarizability. Based on the relation between (n) and the photon energy (E) as shown in Fig. 6(b), there are two types of dispersion: normal dispersion, which presents a direct proportional relation located in the energy range below $1.4\ eV$. The second type of dispersion is the anomalous dispersion for the reverse relation located above $1.4\ eV$. For all samples except CdO, the normal dispersion in the energy range is less than $1.2\ eV$ and the anomalous dispersion is above $1.2\ eV$. The values of k are very small compared with n. The extinction coefficient (k) and refractive index (n)off the nanocomposite decreased as the photon energy (E) increased.

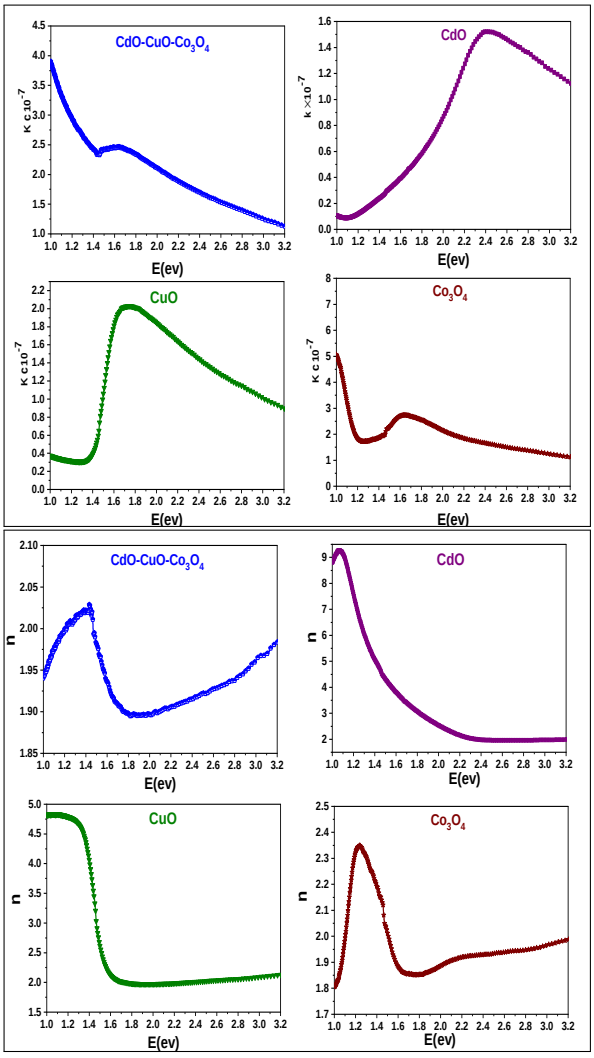

Figure 6. (a): Absorption index (k) of the CdO,CuO,Co_3O_4 (NPs) and CdO-CuO-Co_3O_4 (NC) as a function of the photon energy. (b)Refractive index (n) of the CdO,CuO,Co_3O_4 (NPs) and CdO-CuO-Co_3O_4 (NC) as a function of the photon energy

5.4.3. Optical conductivity

The optical conductivity σ_{opt} is expressed as the optical response of the material to the spreading of charge carriers owing to the excitation caused by the event photon energy. The following equation states that the optical conductivity directly relies on the refractive index and absorption coefficient of the materials [37, 38].

$$\sigma_{opt} = \frac{n\alpha c}{4\pi}, \tag{9}$$

where C is the speed of light in a vacuum. Figure 7 illustrates how the optical conductivity varies with the incident photon energy for CdO, CuO, Co_3O_4 (NPs) and CdO- CuO-Co_3O_4 (NC). Figure 7 shows that the optical

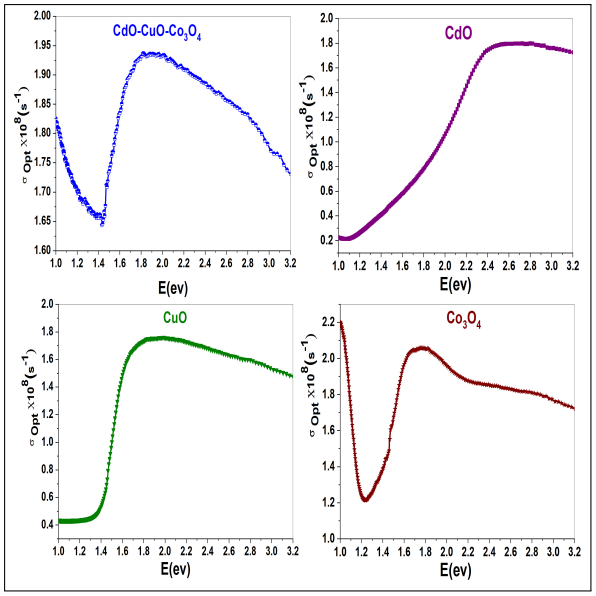

Figure 7. Optical conductivity on the photon energy for CdO,CuO,Co_3O_4 (NPs) and CdO-CuO-Co_3O_4 (NC)

conductivity increases at high photon energies. Owing to the excellent absorbent properties of the nanocomposite in this area, carriers were excited from the valence band to the conduction band, which resulted in higher value of σ_{opt}. It is obvious that the optical conductivity of CdO is between 0.21×10^8 and 1.78×10^8 (S^{-1}) and that the range of photon energies is (1–2.4 $)eV$. The values of optical conductivity of CuO are between 0.42×10^8 and 1.74×10^8 (S^{-1}) and the range of photon energies (1–1.64) eV; the values of optical conductivity of Co_3O_4 are between 1.2×10^8 and 2.06×10^8 (S^{-1}) and the range of photon energies (1.2–1.7) eV; whereas the values of optical conductivity of CdO-CuO-Co_3O_4 (NC) are between 1.65×10^8 and 1.93×10^8 (S^{-1}) and the range of photon energies (1.43–1.82) eV. The highest value of σ_{opt} was observed in the visible regions of CdO,CuO, Co_3O_4 (NPs) and CdO- CuO -Co_3O_4 (NC).

5.5. Electrical studies

The DC electrical resistivity of the samples were studied as a function of temperature. The following equation was used to calculate the DC electrical resistivity (ρ) [39, 40].

$$\rho = \frac{V}{I}\frac{A}{L}, \tag{10}$$

where I is the measured current, V is the applied voltage, L is the pellet thickness, and A is the pellet cross-sectional area. The DC electrical resistivity decreased with the temperature as shown in Fig. 8. This figure shows how the electrical resistivity of the prepared sample changes with temperature. It was observed that the electrical resistivity decreased as the temperature increased, indicating the semiconducting behavior of the sample. It is clear that the mixed (NC) has lower resistivity (higher conductivity) than the single (NPs). This result is in accordance with the results of optical properties, where the lowest band gap energy was for NC; hence, the optical energy gap (Eg) decreases and the electrical conductivity increases. The result is in agreement with Munawar *et al* [29]. The temperature dependence of

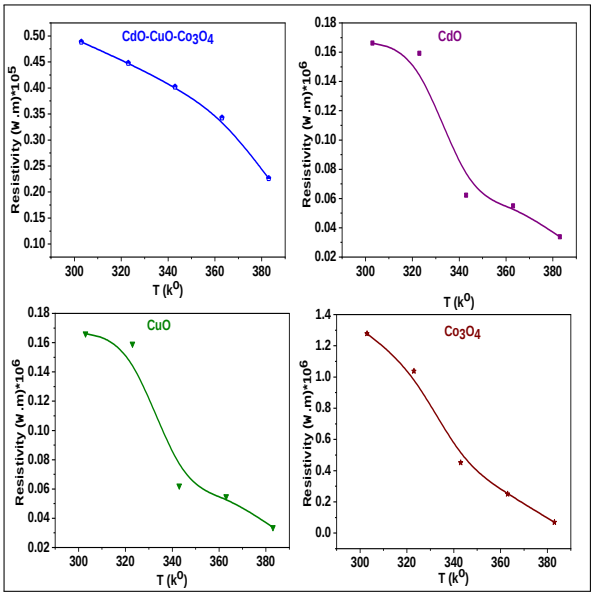

Figure 8. Resistance of the CdO, CuO, Co_3O_4 (NPs) and CdO-CuO-Co_3O_4 (NC) as a function of annealing temperature

the DC resistivityρ_{DC} can be expressed by Arrhenius law [41]:

$$\rho_{DC} = \rho_0 Exp\left(\frac{-E}{k_B T}\right), \tag{11}$$

where ρ_o is a constant, k_B is Boltzmann's constant, T is the temperature in Kelvin, and E is the activation energy.

The activation energies of CdO,CuO,Co_3O_4 and CdO-CuO -Co_3O_4 (NC) were computed from $\ln\sigma$ *and* $1/T$, as shown in Fig. 9, and the obtained values are given in Table 4, which is consistent with previous study results [42–44]. The previous results clearly show that the

Table 4. Values of the activation energies of a CdO, CuO, Co_3O_4 (NPs) and CdO-CuO-Co_3O_4 (NC)

Samples	$E\ (eV)$
CdO	0.183
CuO	0.211
Co_3O_4	0.357
CdO-CuO -Co_3O_4	0.151

activation energy decreased with the mixture.

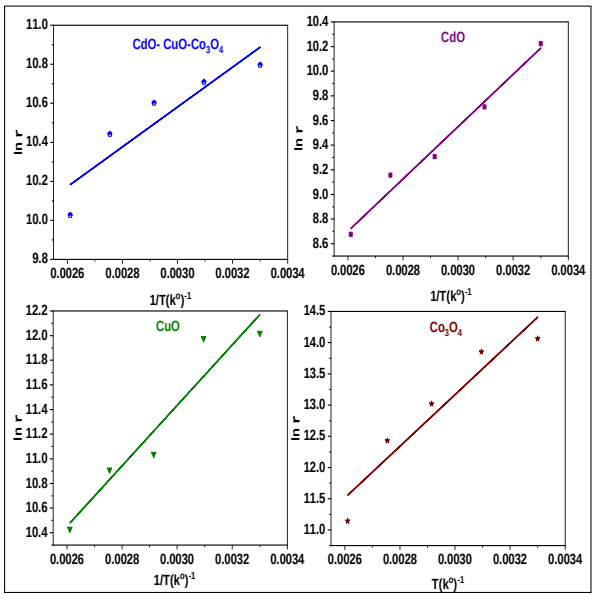

Figure 9. variation of $\ln\rho$ with $\frac{1}{T}\ (k^{-1})$ for the CdO,CuO,Co_3O_4 (NPs) and CdO-CuO-Co_3O_4 (NC) at different temperature of annealing

6. CONCLUSION

CdO, CuO, Co_3O_4 (NPs) and CdO-CuO-Co_3O_4 (NC) were effectively prepared using the co-precipitation method. Cubic structured CdO, Co_3O_4, and monoclinic structured CuO peaks were found in the XRD pattern of the composite. The highest peaks in the XRD patterns were observed for CuO, whereas the lowest peaks were for CdO. The TEM image shows that the particle size of the nanocomposites was $11.4\ nm$. The XRD and TXRF results confirmed the purity of the samples. The optical bandgap of the (NC) is $1.24\ eV$. The DC resistivity measurements showed typical semiconducting behavior for (NPs) and (NC) samples, where the electrical resistivity decreased as the temperature increased.

REFERENCES

[1] M. Subhan and et al., "Photoluminescence, photocatalytic and antibacterial activities of CeO_2·CuO·ZnO nanocomposite fabricated by co-precipitation method," Spectrochimica Acta Part A: Mol. Biomol. Spectrosc. **149**, 839–850 (2015).

[2] S. Das and V. Srivasatava, "Synthesis and characterization of ZnO–MgO nanocomposite by co-precipitation method," Smart Sci. **4**, 190–195 (2016).

[3] S. Thambidurai and et al., "Enhanced bactericidal performance of nickel oxide-zinc oxide nanocomposites synthesized by facile chemical co-precipitation method," J. Alloy. Compd. **830**, 154642 (2020).

[4] D. Paul and et al., "Bi-functional NiO-ZnO nanocomposite: synthesis, characterization, antibacterial and photo assisted degradation study," Adv. Powder Technol. **32**, 131–143 (2021).

[5] N. Abraham and et al., "Dye sensitized solar cells using catalytically active CuO-ZnO nanocomposite synthesized by single step method," Spectrochimica Acta Part A: Mol. Biomol. Spectrosc. **200**, 116–126 (2018).

[6] C. Vidyasagar and et al., "Solid-state synthesis and effect of temperature on optical properties of Cu–ZnO, Cu–CdO and CuO nanoparticles," Powder Technol. **214**, 337–343 (2011).

[7] S. Das and V. Srivastava, "Synthesis and characterization of ZnO/CuO nanocomposite by electrochemical method," Mater. Sci. Semicond. Process. **57**, 173–177 (2017).

[8] A. Sobhani and M. Salavati-Niasari, "Synthesis and characterization of $FeSe_2$ nanoparticles and $FeSe_2$/FeO(OH) nanocomposites by hydrothermal method," J. Alloy. Compd. **625**, 26–33 (2015).

[9] Q. e. a. Wang, "Synthesis of (ZrO_2-Al_2O_3)/GO nanocomposite by sonochemical method and the mechanism analysis of its high defluoridation," J. Hazard. Mater. **381**, 120954 (2020).

[10] S. Amiri and A. Rahimi, "Hybrid nanocomposite coating by sol–gel method: A review," Iran. Polym. J. **25**, 559–577 (2016).

[11] S. Gierlotka *et al.*, "Synthesis of metal-ceramic nanocomposites by high-pressure infiltration," Solid State Phenom. **101**, 157–164 (2004).

[12] K. Vidal *et al.*, "Characterization of LaNi0.6Fe0.4O_3 perovskite synthesized by glycine-nitrate combustion method," Solid State Ionics **269**, 24–29 (2015).

[13] T. Thilagavathi *et al.*, "WO_3/$CoWO_4$ nanocomposite synthesis using a facile co-precipitation method for enhanced photocatalytic applications," J. Phys. Chem. Solids **154**, 110066 (2021).

[14] D. Chhikara, K. Srivatsa, and S. Muthusamy, "On the synthesis and characterization of ZnO/MgO nanocomposite by thermal evaporation technique," Solid state sciences **37**, 108–113 (2014).

[15] T. Munawar *et al.*, "Synthesis of novel heterostructured ZnO-CdO-CuO nanocomposite: characterization and enhanced sunlight driven photocatalytic activity," Mater. Chem. Phys. **249**, 122983 (2020).

[16] N. Thovhogi *et al.*, "Physical properties of CdO nanoparticles synthesized by green chemistry via hibiscus sabdariffa flower extract," J. Alloy. Compd. **655**, 314–320 (2016).

[17] K. Karthik *et al.*, "Photocatalytic and antibacterial activities of hydrothermally prepared CdO nanoparticles," J. Mater. Sci. Mater. Electron. **28**, 11420–11429 (2017).

[18] N. Al-Hada *et al.*, "A facile thermal-treatment route to synthesize the semiconductor CdO nanoparticles and effect of calcination," Mater. science semiconductor processing **26**, 460–466 (2014).

[19] S. Reddy *et al.*, "Synthesis of CdO nanoparticles and their modified carbon paste electrode for determination of dopamine and ascorbic acid by using cyclic voltammetry technique," Int. J. Electrochem. Sci **5**, 10–17 (2010).

[20] M. Grigore *et al.*, "Methods of synthesis, properties and biomedical applications of CuO nanoparticles," Pharmaceuticals **9**, 75 (2016).

[21] H. Wang *et al.*, "Preparation of CuO nanoparticles by microwave irradiation," J. crystal growth **244**, 88–94 (2002).

[22] A. Radhakrishnan and B. Beena, "Structural and optical absorption analysis of CuO nanoparticles," Indian J. Adv. Chem.

Sci **2**, 158–161 (2014).
[23] K. Reddy, "Green synthesis, morphological and optical studies of CuO nanoparticles," J. Mol. Struct. **1150**, 553–557 (2017).
[24] M. Salavati-Niasari and A. Khansari, "Synthesis and characterization of Co_3O_4 nanoparticles by a simple method," Comptes Rendus Chimie **17**, 352–358 (2014).
[25] R. Bhargava *et al.*, "Investigation of structural, optical and electrical properties of Co_3O_4 nanoparticles," in *AIP conference proceedings,* (AIP Publishing LLC, 2018).
[26] D. Letsholathebe *et al.*, "Optical and structural stability of Co_3O_4 nanoparticles for photocatalytic applications," Mater. Today: Proc. **36**, 499–503 (2021).
[27] T. Aldeen, H. Mohamed, and M. Maaza, "Bio-inspired single phase monteponite CdO nanoparticles via natural extract of phoenix roebelenii palm leaves," J. Inorg. Organomet. Polym. Mater. **30**, 4691–4701 (2020).
[28] A. Ahmed *et al.*, "Effect of ethylene glycol concentration on the structural and optical properties of multimetal oxide CdO–NiO–Fe_2O_3 nanocomposites for antibacterial activity," J. Phys. Chem. Solids **155**, 110113 (2021).
[29] T. Munawar *et al.*, "Multi metal oxide NiO-Cdo-ZnO nanocomposite–synthesis, structural, optical, electrical properties and enhanced sunlight driven photocatalytic activity," Ceram. Int. **46**, 2421–2437 (2020).
[30] J. Ma *et al.*, "Visible-light photocatalytic decolorization of orange II on Cu_2O/ZnO nanocomposites," Ceram. Int. **41**, 2050–2056 (2015).
[31] S. Balamurugan *et al.*, "Multi metal oxide CdO–Al_2O_3–NiO nanocomposite—synthesis, photocatalytic and magnetic properties," Mater. research express **6**, 015022 (2018).
[32] A. Ahmed *et al.*, "Improvement of the crystallinity and photocatalytic property of zinc oxide as calcination product of Zn–AL layered double hydroxide," J. alloys compounds **539**, 154–160 (2012).
[33] M. Ishfaq *et al.*, "Wet-chemical synthesis of ZnO/CdO/CeO_2 heterostructure: a novel material for environmental remediation application," Ceram. Int. **48**, 34590–34601 (2022).
[34] D. Gupta *et al.*, "Facile synthesis of Cu_2O and CuO nanoparticles and study of their structural, optical and electronic properties," J. Alloy. Compd. **743**, 737–745 (2018).
[35] M. Nassar and I. Ahmed, "Hydrothermal synthesis of cobalt carbonates using different counter ions: An efficient precursor to nano-sized cobalt oxide (Co_3O_4)," Polyhedron **30**, 2431–2437 (2011).
[36] A. Ahmed *et al.*, "Magnetic and optical properties of synthesized ZnO–$ZnFe_2O_4$ nanocomposites via calcined Zn–Fe layered double hydroxide," Opt. Mater. **108**, 110179 (2020).
[37] T. Soliman and S. Vshivkov, "Effect of fe nanoparticles on the structure and optical properties of polyvinyl alcohol nanocomposite films," J. Non-Crystalline Solids **519**, 1194522019 (2019).
[38] S. Gad and A. Moez, "Enhanced optical conductivity, nonlinear optical and semiconducting properties of Mg 1 x Cu x O/PMMA Nanocomposite," J. Inorg. Organomet. Polym. Mater. **30**, 469–476 (2020).
[39] V. Nithya and R. Selvan, "Synthesis, electrical and dielectric properties of $FeVO_4$ nanoparticles," Phys. B: Condens. Matter **406**, 24–29 (2011).
[40] S. Yousaf *et al.*, "Tuning the structural, optical and electrical properties of NiO nanoparticles prepared by wet chemical route," Ceram. Int. **46**, 3750–3758 (2020).
[41] S. Singhal *et al.*, "Cu-doped ZnO nanoparticles: synthesis, structural and electrical properties," Phys. B: Condens. Matter **407**, 1223–1226 (2012).
[42] R. Tripathi *et al.*, "Dielectric relaxation of CdO nanoparticles," Appl. Nanosci. **6**, 175–181 (2016).
[43] H. Bitra *et al.*, "Synthesis and enhanced dielectric properties of copper oxidenanoparticles," Mater. Chem. Phys. **254**, 123379 (2020).
[44] S. Srijith *et al.*, "Structural and electrical characterization of cobalt oxide nanoparticles," Mater. Chem. Phys. **01**, 07–15 (2023).